Vibrational sum-frequency generation spectroscopy of lipid bilayers at repetition rates up to 100 kHz ⊕

Freeda Yesudas; Mark Mero; Janina Kneipp; ... et. al

Check for updates

CrossMark

View Online   Export Citation

Articles You May Be Interested In

Lipid and lipid-polymer mixtures at an interface

AIP Conference Proceedings (June 2000)

Compact, high-repetition-rate source for broadband sum-frequency generation spectroscopy

APL Photonics (May 2017)

Spectral assignment and orientational analysis in a vibrational sum frequency generation study of DPPC monolayers at the air/water interface

J. Chem. Phys. (December 2016)

AIP Publishing

Vibrational sum-frequency generation spectroscopy of lipid bilayers at repetition rates up to 100 kHz

Freeda Yesudas,[1,2] Mark Mero,[3] Janina Kneipp,[1,2] and Zsuzsanna Heiner[1,2,a]

[1]*School of Analytical Sciences Adlershof, Humboldt Universität zu Berlin, Albert-Einstein-Str. 5-11, 12489 Berlin, Germany*
[2]*Department of Chemistry, Humboldt Universität zu Berlin, Brook-Taylor-Str. 2, 12489 Berlin, Germany*
[3]*Max Born Institute for Nonlinear Optics and Short Pulse Spectroscopy, Max-Born-Str. 2a, 12489 Berlin, Germany*

Broadband vibrational sum-frequency generation (BB-VSFG) spectroscopy has become a well-established surface analytical tool capable of identifying the orientation and structure of molecular layers. A straightforward way to boost the sensitivity of the technique could be to increase the laser repetition rate beyond that of standard BB-VSFG spectrometers, which rely on Ti:sapphire lasers operating at repetition rates of 1-5 kHz. Nevertheless, possible thermally induced artifacts in the vibrational spectra due to higher laser average powers are unexplored. Here, we discuss laser power induced temperature accumulation effects that distort the BB-VSFG spectra of 1,2-diacyl-*sn*-glycero-3-phosphocholine at an interface between two transparent phases at repetition rates of 5, 10, 50, and 100 kHz at constant pulse energy. No heat-induced distortions were found in the spectra, suggesting that the increase in the laser repetition rate provides a feasible route to an improved signal-to-noise ratio or shorter data acquisition times in BB-VSFG spectroscopy for thin films on transparent substrates. The results have implications for future BB-VSFG spectrometers pushing the detection limit for molecular layers with low surface coverage. © 2018 Author(s). *All article content, except where otherwise noted, is licensed under a Creative Commons Attribution (CC BY) license (http://creativecommons.org/licenses/by/4.0/).* https://doi.org/10.1063/1.5016629

INTRODUCTION

Broadband vibrational sum frequency generation (BB-VSFG) spectroscopy is a powerful surface-specific tool to study the composition, orientation, interaction, and dynamics of molecules at interfaces.[1–5] Phospholipids are frequently studied by BB-VSFG spectroscopy, as they are vital constituents of all biological cells, organelles, and other biological compartments.[6] As the investigation of lipids has gained increasing importance because of their broad biomedical applications, BB-VSFG spectra of lipid bilayers have been studied at different interfaces, e.g., solid/water,[7,8] air/water,[9–11] or solid/air[8,12,13] interfaces, usually at laser repetition rates of 1 kHz.

Although BB-VSFG spectroscopy can reach sub-monolayer sensitivity, a further two to three-order of magnitude improvement in sensitivity is essential to detect and analyze biomolecules at small surface coverages.[1] Enhancing the stability and/or increasing the repetition rate of laser sources can provide the required boost in signal-to-noise ratio (SNR) in BB-VSFG measurements.[14–16] Recently, we have reported the development of the first 100-kHz BB-VSFG spectrometer that can serve to study biomolecules in the spectral region between 2800 and 3600 cm^{-1}, where the fundamental stretching modes of O–H, N–H, and C–H bonds lie.[17] A major

drawback of high-repetition-rate laser sources is that the corresponding high average laser powers at a given pulse energy may lead to thermally induced effects, as was reported, e.g., for lipids, which showed gauche defects, disorder, or phase transitions that modify the vibrational signature of the layers to be studied.[18–21] Such effects can be severe, in particular, with strongly absorbing substrates, such as water, even at the standard laser repetition rate of 1 kHz.[18] Nevertheless, due to lack of systematic investigations of thermal effects as a function of (i) the laser repetition rate and (ii) the absorption properties of the substrate and the investigated molecular layer, the laser parameter range, where reliable, *in situ* vibrational spectral data can be collected, is poorly understood.

As a first step, we demonstrate here the feasibility of BB-VSFG experiments covering the range of vibrational resonances of the alkyl chains of phospholipids at repetition rates well above 1 kHz up to 100 kHz for the restrictive case, where the absorptive layer is between two transparent phases. Specifically, we investigated the dependence of the vibrational spectra of lipid bilayers at a CaF$_2$/air interface on the repetition rate. CaF$_2$ is an ideal substrate material for such a study, as it is transparent both in the mid-infrared (MIR) and the visible (VIS) spectral range, and possible thermal effects are expected to arise due to the MIR laser energy absorbed solely in the lipid layer. We discuss characteristic fingerprints of phosphatidylcholine, spectral averaging and signal-to-noise ratio, the stability of the intensity of vibrational bands at varying repetition rate and under prolonged excitation, and the

---

a)Author to whom correspondence should be addressed: heinerzs@hu-berlin.de

predictions of an analytical 3D heat diffusion model. As will be demonstrated, our results have implications for future high repetition rate BB-VSFG studies on model membranes and real biological samples.

MATERIALS AND METHODS

Preparation of lipid bilayers

Lyophilized powder of 1,2-diacyl-*sn*-glycero-3-phosphocholine (PC, 99%) was purchased from Sigma-Aldrich (Munich, Germany). A protocol known to yield unilamellar vesicles was applied according to Ref. 22. Briefly, a 50-mM lipid solution was prepared in chloroform: methanol (Merck) at a ratio of 1:1 (v:v). The suspension was dried in a glass tube by a stream of nitrogen. Resuspension of the lipids in phosphate-buffered saline (PBS, pH 7.4) was followed by vortexing. The procedure was repeated through five freeze/thaw cycles, and the lipid dispersion was extruded 17 times through two polycarbonate membranes of 100 nm pore size using a mini-extruder (Avanti Polar Lipids, Inc.). The final concentration of the lipid vesicle dispersion was 7 mM in PBS buffer. CaF_2 (110) windows were cleaned with toluene (Merck), ethanol (Merck), and finally with Millipore water (18 MΩ) for 10 min in each solvent. As a next step, oxygen plasma cleaning was employed to remove remaining solvent directly before application of the lipids. This procedure is known to increase hydrophilicity of the CaF_2 surface.[23] The lipid dispersion was again dissolved in water in the ratio of 1:10, sonicated, injected on the surface of CaF_2 using the vesicle fusion method,[24,25] and dried at room temperature.

Experimental setup

The layout of the system is shown in Fig. 1(a). Details regarding the performance of the experimental configuration were described recently.[17] Briefly, the home-built light source consists of (i) a two-stage optical parametric amplifier (OPA) system providing few-cycle pulses at 1.5 μm and 3.2 μm and (ii) a sum frequency generation stage providing transform-limited narrowband, picosecond pulses at ~515 nm. The pump source driving the whole system is a compact, commercial Yb-laser (Pharos, Light Conversion Ltd.) operating at a repetition rate of 100 kHz. In addition to the high repetition rate, the source also exhibits high power stability. The corresponding

RMS value measured for the MIR beamline is 0.27% over a two-hour period.[17]

In the BB-VSFG setup, the 60-fs MIR pulses and the 4.5-ps VIS pulses were focused onto the sample surface using an f = 50 mm and an f = 300 mm lens, respectively. The angle of incidence, beam waist, and incident pulse energy of the MIR and VIS pulses was 57°, 20 μm, 0.55 μJ and 68°, 150 μm, 4.25 μJ, respectively. The generated sum-frequency signal was imaged onto the slit of a 320-mm spectrograph equipped with a Peltier-cooled, back-illuminated, deep-depletion CCD (Horiba, Synapse).

The up-converted spectrum of the MIR laser beam was obtained using an air-gold interface at zero delay [cf. Fig. 1(b), red curve]. The full width at half maximum (FWHM) of the visible pulse is 3 cm^{-1} [Fig. 1(b), green curve], which defines the spectral resolution of our measurements. In all experiments, both the MIR and the visible pulse peak power were kept constant. We used zero-order waveplates to control the polarizations of the excitation pulses and a polarizer for selecting a particular polarization component of the generated SFG signal relative to the plane of incidence on the sample (i.e., p: parallel, s: perpendicular). All measurements were taken in ppp, ssp, pss, and sps polarization combinations for the SFG, visible, and MIR beams, respectively. In order to control the acquisition times and to turn each beam ON or OFF, fast mechanical shutters were used. The measurements were taken at room temperature (23 °C) and 32% humidity. In our experiments, we used the so-called "window geometry"[13,26] with the VIS and MIR laser beams falling on an air-solid interface, as opposed to the "prism geometry,"[13,15,27] where the VIS and MIR beams would be incident on a solid-air interface involving total internal reflection. As is well known, the vibrational spectra measured using the "window geometry" are different from the vibrational spectra obtained in the "prism geometry" due to the different Fresnel coefficients in the two cases.[13]

Data pre-processing

Each sum-frequency spectrum was first frequency calibrated using the well-known absorption spectrum of a 50-μm-thick polystyrene film inserted in the MIR beam and cosmic spikes were removed. Following cosmic spike removal, the difference spectrum was calculated by subtracting the background spectrum (i.e., no MIR laser excitation) from the raw
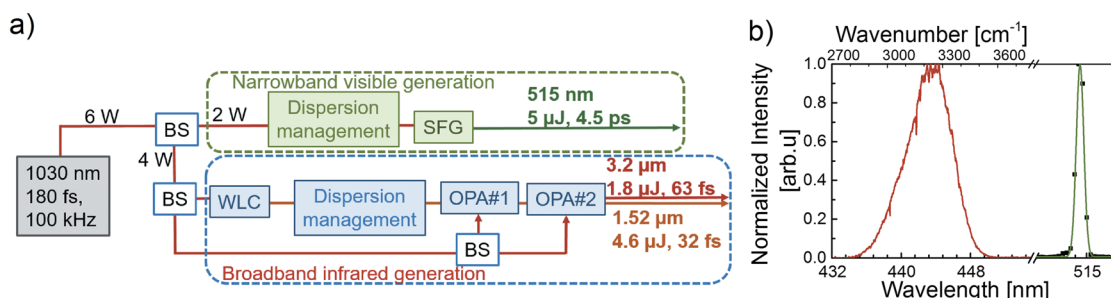
FIG. 1. (a) Schematic layout of the BB-VSFG light source. BS: beam splitter, SFG: sum-frequency (ps visible pulse) generation, OPA#1 and OPA#2: first and second stage of the optical parametric amplifier, WLC: white light continuum generation. (b) Normalized BB-VSFG spectrum from a Au (111) surface (red) and normalized spectrum of a narrowband visible pulse (black symbols) and the fitted Gaussian with a FWHM of 3 cm^{-1}.

spectrum. The non-resonant SFG spectrum obtained from a Au (111) surface was used to normalize the difference BB-VSFG spectrum. All normalizations were taken without averaging, smoothing, or any other data pre-processing. All spectra were analyzed using MATLAB (The Mathworks, Inc., Ismaning, Germany) and Origin (OriginLab, Northampton, MA) software.

RESULTS AND DISCUSSION

Using lipid bilayers obtained from phosphatidylcholine on the CaF_2 interface, we recorded BB-VSFG spectra at the CaF_2/air interface in the C–H stretching region from 2800 cm^{-1} to 3600 cm^{-1}. Two sets of experiments were conducted. First, we measured the dependence of the signal to noise ratio (SNR) as a function of laser repetition rate and signal averaging. In the second set of experiments, we monitored the stability of the peak count of characteristic spectral bands over time at repetition rates ranging from 5 kHz to 100 kHz. The BB-VSFG spectra were recorded in all relevant polarization combinations, i.e., ppp, ssp, pss, and sps, which allow the determination of molecular orientation, orientation order, hyperpolarizability ratio, or even interfacial refractive index in certain cases.[28,29] Using a simple analytical 3D heat diffusion model, we simulate the accumulated temperature rise as a function of repetition rate for the conditions of our experiments.

BB-VSFG spectra of phospholipids at a repetition rate of 100 kHz

To obtain reliable VSFG spectra, two main technical issues have to be resolved: (i) suppression of the non-resonant background and (ii) keeping the distortions and broadening in the spectral lines to a minimum. On the one hand, the interference of the resonant and non-resonant (NR) signals in VSFG provides an opportunity for absolute molecular orientation analysis.[30] On the other hand, the non-resonant signal can distort or overwhelm the resonant signal in certain cases, which then prevents the successful interpretation of the spectra.[31–33] In addition, a MIR-VIS time delay can further distort the spectra.[34–36] Even though the NR background is small on dielectrics, we determined an optimal time delay between the MIR and VIS pulses in order to minimize the non-resonant background after confirming that spectral distortions caused by phase differences between neighboring vibrational bands do not occur in our delay range (see the supplementary material). In Figs. 2(a) and 2(b), the raw VSFG spectra of PC at a

CaF$_2$/air interface are shown for different time delays between 0 and 3 ps. Figures 2(a) and 2(b) show the spectra recorded in ppp and ssp polarization combinations, respectively (see the section titled Materials and Methods for further information). The spectra in Fig. 2 indicate a decrease in the VSFG intensity, as the delay of the VIS pulse relative to the MIR pulse increased, while peak position and spectral linewidth at each delay remained the same. From the spectra in Fig. 2(a), we concluded that a 666-fs time delay is an optimum because the non-resonant background was slightly lower but the signal intensity remained high. Our observation is in accord with previous reports.[32,33,37,38] The finite bandwidth and the temporal shape (e.g., asymmetric) of the visible pulse may cause spectral broadening and artifacts in the obtained vibrational spectral shape.[1,37] In our case, the spectral distortions were kept at a minimum, thanks to the chirped sum-frequency generation scheme, which produces extremely narrowband visible spectra with a full width at half maximum (FWHM) of ~3 cm^{-1} [cf. Fig. 1(a)] with symmetric profiles both in the temporal and spectral domain in contrast to common spectral narrowing methods such as using an etalon. A ps VIS probe pulse with our spectral FWHM causes less than 1 cm^{-1} broadening for our extracted Lorentzian vibrational spectral bands (c.f. the supplementary material). Therefore, we consider both effects negligible here.

Figure 3(a) shows normalized BB-VSFG spectra acquired over a single, 10 s time period where the VIS pulse was delayed with respect to the MIR pulse by 666 fs for all four polarization combinations. Vibrational spectra recorded in different polarization combinations provide access to different elements or element combinations of the hyperpolarizability tensor of a particular molecular group in a well-ordered molecular layer.[30] The assignments of the vibrational bands obtained from fitting Lorentzian line profiles for the sample are summarized in Table I (for more details, please see the supplementary material).

The vibrational bands observed in our experiments show good agreement with spectra of the lipids reported before.[12,28,39] The spectrum obtained at ppp polarization [Fig. 3(a), black] contains one dominant peak assigned to the methyl asymmetric C–H stretch (CH$_{3-as}$) at 2969 cm^{-1}, furthermore the methyl symmetric C–H stretch (CH$_{3-s}$) appears at 2879 cm^{-1} together with an additional, broad feature between 2895 and 2920 cm^{-1} with peaks at 2902 and 2914 cm^{-1}, which may be due to the methylene asymmetric C–H stretch (CH$_{2-as}$) and its Fermi resonance (CH$_{2-FR}$), respectively.[12] A spectral shoulder, appearing in ppp polarization configuration at 2940 cm^{-1}, is the Fermi resonance of the methyl group of the
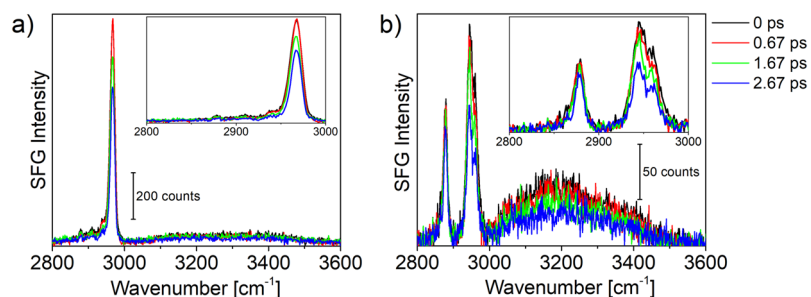
FIG. 2. Raw BB-VSFG spectra of phosphatidylcholine on a CaF$_2$ plate using (a) ppp and (b) ssp polarization combination at different delays between MIR and VIS pulses: 0 fs (black), 666 fs (red), 1.66 ps (green), and 2.66 ps (blue). Integration time was 10 s, without further averaging, at a repetition rate of 100 kHz.
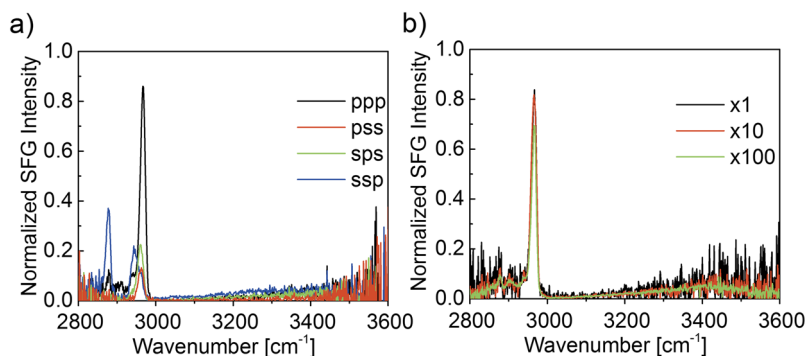
FIG. 3. (a) Normalized BB-VSFG spectra of phosphatidylcholine on a CaF$_2$ plate using ppp, ssp, sps, pss polarization at 100 kHz, obtained with 10 s acquisition time without further averaging. (b) Impact of averaging on the normalized SFG spectra: single, 10-s collected spectrum (black), average of 10 spectra at 10-s (red) and average of 100 spectra at 10-s (green) integration time using ppp polarization combination.

CH$_3$ symmetric stretch and the C–H bending overtone.[12,28,30] The ssp configuration [Fig. 3(a), blue] shows two prominent bands: the symmetric methyl stretch (CH$_{3-s}$) at 2879 cm^{-1} which is the highest peak in this polarization combination using "window geometry" and a Fermi resonance (CH$_{3-FR}$) at 2940 cm^{-1} of the CH$_{3-s}$ stretching and the methyl bending (1375 cm^{-1}) modes as it was also observed in Refs. 12 and 13. In addition to the two prominent bands, in ssp polarization, a shoulder also becomes visible with a peak at 2964 cm^{-1} that was assigned previously as the center frequency of the in-plane asymmetric stretching mode of the methyl groups (CH$_{3-as}$).[40] The sps peak in Fig. 3(a) (marked green) is centered at ~2960 cm^{-1} and is clearly red-shifted compared to the peak at ~2963 cm^{-1} as well as the peak at 2969 cm^{-1} observed in pss and ppp polarization combinations, respectively. This ssp/ppp splitting of the CH$_3$ asymmetric stretching mode of the methyl group provides spectral evidence for the lift of the degeneracy between the in-plane and out-of-plane vibrations.[9,40,41] Furthermore, the in-plane mode can only be detected in sps polarization, while the ssp and ppp combinations are insensitive to this vibration.[40]

In ssp polarization, the intensity of the band of the symmetric methyl stretch is higher than that of the corresponding Fermi resonance [Fig. 3(a), blue]. In addition, the intensity of the asymmetric methyl stretch in ssp polarization is weaker than in sps polarization [Fig. 3(a), blue versus green, respectively] suggesting that the CH$_3$ tilt angle is smaller than 45° with respect to the surface normal.[28,39] As can be seen in Fig. 3(a), the vibrational bands of the methylene (CH$_2$) group (i.e., broad feature at 2900-2920 cm^{-1}) are much weaker than that of the methyl group (i.e., bands at 2940 cm^{-1} and

2964/2969 cm^{-1}). In all-trans conformation, the CH$_{2-s}$ signal must be absent from the spectra due to the inversion symmetry of the layer. Thus, tightly packed lipids will show CH$_{3-s}$ and CH$_{3-FR}$ vibrations with only very small or no CH$_2$ bands in ssp polarization.[12] The experimental results shown here prove that the lipids prepared from vesicles are well ordered or only very slightly disordered on the surface of the CaF$_2$ substrate. A more detailed analysis of tilt angle of the methyl group will be the subject of a future study.

Figure 3(b) shows three normalized VSFG spectra at ppp polarization collected at 100 kHz that are averages of 1, 10, and 100 individual spectra, respectively. The low SNR in the single spectrum [Fig. 3(b), black trace] at the edges of our spectral window, and also in the spectra of Fig. 3(a) discussed above is due to the low MIR spectral energy density at 2800 cm^{-1} and 3600 cm^{-1} and that these spectra were taken with a single, 10-s acquisition time. Our BB-VSFG spectrometer driven with a 100-kHz laser has high potential to decrease the integration time without sacrificing the signal to noise ratio.[15] While the black curve in Fig. 3(b) corresponds to a single, 10-s integration time window, the red and green curve show VSFG spectra averaged 10 and 100 times. The corresponding SNR was 80, 190, and 500 for 1, 10, and 100 times averaged, 10-s spectra, respectively. For the SNR estimate, the signal was taken as the peak value of the 2965-cm^{-1} band (where the influence of neighboring bands is minor in ppp polarization combination) after background correction and normalization by the measured, background-corrected, single non-resonant spectrum (without averaging or smoothing) recorded on a gold surface, while the noise was determined in the spectral range of 3000-3100 cm^{-1}.[42] The noise in the reference spectrum was 0.01% and was considered negligible. The signal to noise ratio in the 100 times averaged case (ca. 16 min) remains high in the full 800-cm^{-1} spectral window of our MIR excitation pulse.

VSFG signal stability and repetition rate dependence

Each of the four different panels in Fig. 4 shows spectra from the same samples, yet at decreasing repetition rates of 100, 50, 10, and 5 kHz, respectively [Figs. 4(a)–4(d), respectively]. An integrated pulse picker in the commercial pump laser made it possible to continuously adjust the repetition rate without altering the pulse energy. At each repetition rate, the acquisition time in the VSFG experiment was adjusted to keep the number of laser shots constant. As a result, the average power reaching the sample decreased proportionally

TABLE I. Vibrational SFG wavenumbers and the corresponding band assignments of the CH stretching modes of phosphatidylcholine in the region of 2800 cm^{-1} and 3000 cm^{-1}. s: symmetric stretching, as: asymmetric stretching, FR: Fermi resonance.

Assignments	VSFG wavenumber (cm^{-1})	References
CH$_{3-s}$	2879	12, 28, and 39
CH$_{2-as}$	2902	12, 28, and 39
CH$_{2-FR}$	2914	12, 28, and 39
CH$_{3-FR}$	2940	12, 28, and 39
CH$_{3-as}$	2964[a]	12, 28, and 39

[a]2969 cm^{-1} in ppp, 2964 cm^{-1} ssp, while 2960 cm^{-1} in sps and 2963 cm^{-1} in pss polarization combination. The resonance frequency of each band is the average of the corresponding frequencies in all four measured polarization combinations except for the case of the CH$_{3-as}$ band.
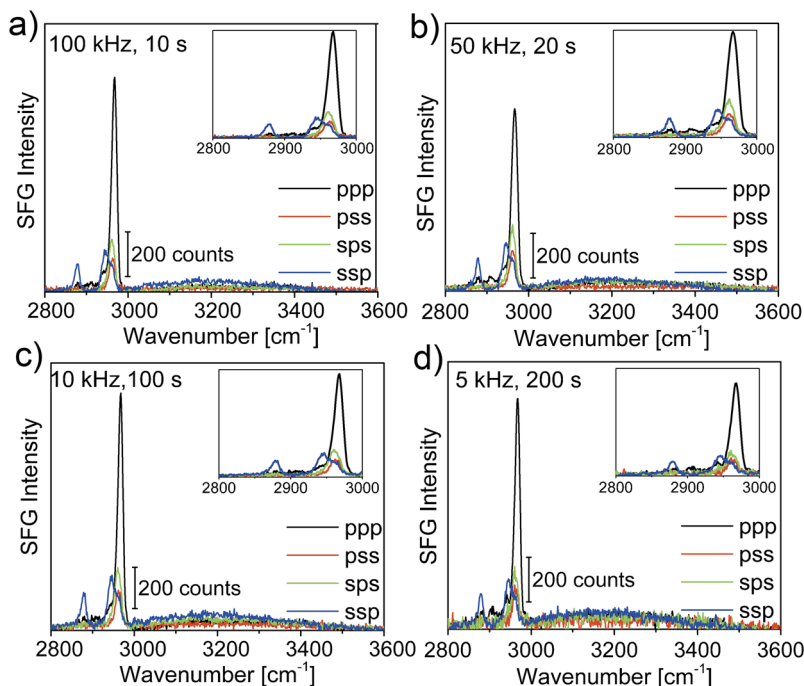
FIG. 4. Raw BB-VSFG spectra of phosphatidylcholine on a CaF_2 plate recorded at ppp (black), pss (red), sps (green), and ssp (blue) polarization combination with 666 fs delay between MIR and VIS pulses (a) at 100-kHz, 10-s; (b) 50-kHz, 20-s; (c) 10-kHz, 100-s; (d) 5-kHz, 200-s repetition rate and acquisition time, respectively, without further averaging.

with the repetition rate. For example, at a repetition rate of 5 kHz, the MIR and VIS average powers were only 2.75 mW and 21 mW, respectively. The SNR of VSFG spectra acquired for 10^6 shots was 37, 50, 55, and 76 at a repetition rate of 5, 10, 50, and 100 kHz, respectively. The result shows that the SNR increases with the repetition rate in spite of a constant number of pulses and pulse energies incident on the sample (cf. Fig. 4). We attribute the higher SNR at higher repetition rates to the lower accumulated dark noise of our CCD at shorter integration times. We note that the accumulated dark noise can be reduced using other types of CCD camera (i.e., iCCD, iEMCCD). The average background count was 1.5 $\times 10^3$ at low repetition rates [5 and 10 kHz, Figs. 4(d) and 4(c), respectively] that decreased to $\sim 10^3$ at 100 kHz [Fig. 4(a)]. The total noise, dark current noise, and readout noise added in quadrature were about 5.5 e^- per pixel RMS over a 200-s acquisition time [corresponding spectra shown in Fig. 4(d)] and decreased to 4.057 e^- per pixel over a 10-s integration time [corresponding spectra shown in Fig. 4(a)]. We note that while the applied maximum average power in our experiments at 100 kHz is a few times higher than the corresponding values in typical experiments conducted at 1-5 kHz repetition rates,[43] the pulse energies are a few 10 times lower. For example, at a repetition rate of 5 kHz, we conducted our measurements with average powers of 2.75/21 mW (MIR/VIS), while in the

literature, 20/215 mW (MIR/VIS) were usually applied. At a repetition rate of 5 kHz, we achieved SNR's (37 in single-shot acquisition and 129 in the case of average of ten spectra at 200-s integration time) approaching those in the literature (SNR: 110-170 at 5 kHz and 5-min acquisition time),[3,42,43] but using an order of magnitude lower average power and shorter integration times.

The spectra in Fig. 4 show highly ordered surface conformation at each repetition rate, i.e., (i) the amplitude and width of the CH_3 bands remain largely unaffected and (ii) the SF signal from the CH_2 vibrations remains small (indicating an unchanged contribution from gauche defects) as the average power increases. Fitting of the spectra in ppp polarization combination leads to approximately the same resonance parameters independent of the average power (see the supplementary material) suggesting negligible heat-induced spectral distortions even at the highest repetition rate.

To monitor the laser-induced heating effects, the spectral intensity of the different C–H stretching bands was monitored over time. The VSFG spectra of PC on CaF_2 were recorded repeatedly with an integration time of 10 s during a time interval of 20 min. The time dependence of the spectral peaks was collected using ssp and ppp polarization combinations. Figure 5(a) shows several VSFG band peak intensities as a function of time measured, while both beams were
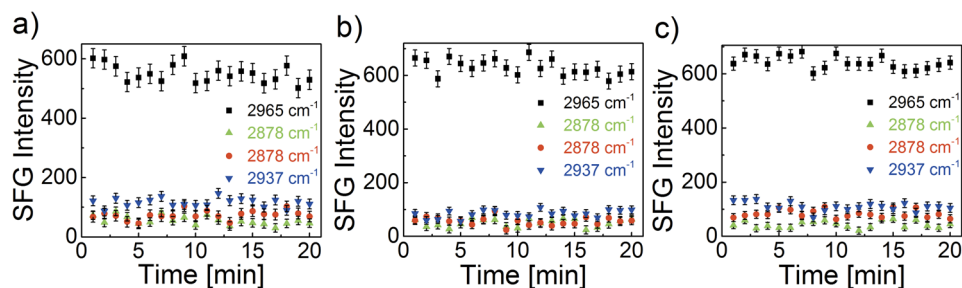
FIG. 5. BB-VSFG intensity fluctuations over time using ppp and ssp polarization at 100 kHz. (a) Both MIR and VIS beams were simultaneously switched ON and OFF. During the measurements, (b) MIR and (c) VIS pulses were continuously ON, while the other beam was only switched ON during the observation. Integration time was 10 s, without further averaging.
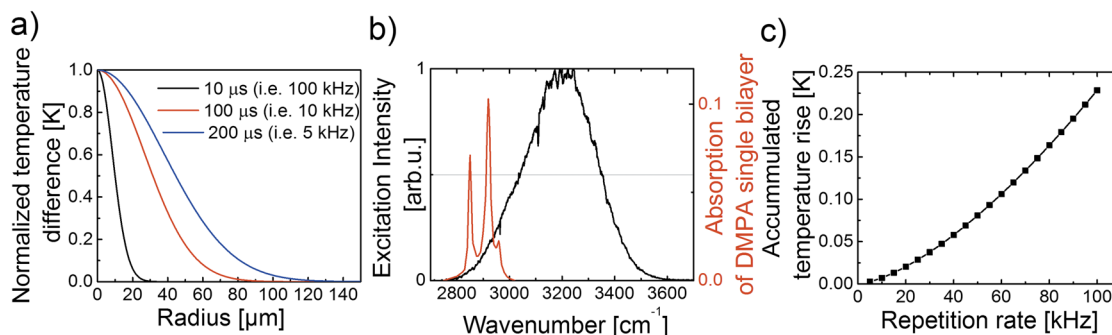
FIG. 6. (a) Normalized temperature increase as a function of distance from the point-like heat source at various times after excitation. (b) Normalized MIR excitation spectrum (black, left axis) and absorption spectrum of DMPA (red, right axis). (c) Accumulated temperature rise at the location of the point-like heat source during laser excitation at repetition rates between 5 and 100 kHz.

simultaneously switched ON and OFF during the measurements. In Fig. 5(b), the fluctuation of the peak intensities of the bands is displayed when the MIR beam was continuously ON and the VIS was only kept ON during the actual spectral acquisition.

Figure 5(c) shows the reverse, i.e., when the visible beam was always ON and the MIR beam was switched ON and OFF for collecting the spectra. The error bars represent the RMS fluctuation in the peak value in the whole 20-min period. We observed no correlation between the various illumination conditions and the fluctuation in peak intensities (i.e., peak count values) and the peak spectral positions. The peak intensities of the different bands and the ratio of the amplitudes of the methyl bands stay constant during the experiments suggesting that no laser-induced damage/heating appears up to a 100-kHz repetition rate. Previous studies show that in ssp polarization, an extra CH_2 signal appears while the CH_3 band weakens due to the more disordered tails and higher number of gauche defects when thermal effects are significant.[18] As no change was found in the SFG signal, we conclude that thermal effects on the structure of the lipid bilayers are negligible or completely absent under our experimental conditions.

Modelling of heat accumulation effects

In order to estimate the temperature rise in the PC layer due to repetitive MIR laser excitation, we employed an analytical solution to 3D heat flow in an infinite half-space[44,45] bounded by an air-PC-CaF$_2$ interface. The thermal resistance of the PC-CaF$_2$ interface and convection cooling at the air-PC interface were neglected. The material properties are assumed to be independent of temperature. The deposited laser energy was considered an instantaneous point-like heat source within the PC layer. The thermal diffusion lengths (i.e., half width of the spatial temperature profile) predicted by the model are 10-44 μm within a time of 10-200 μs [cf. Fig. 6(a)] and are comparable to our MIR laser beam waist of ~20 μm, thereby justifying the validity of the 3D approximation. Due to the lack of absorbance data on PC layers in our MIR excitation range, we used the absorbance as a function of wavenumber data obtained for single bilayers of dimyristoylphosphatidic acid (DMPA),[46] which is a molecule with MIR absorption properties very similar to that of PC. The fraction of laser pulse energy absorbed in the lipid layer was estimated by taking the

ratio of (i) the integral of the product of the absorption spectrum of DMPA and the MIR excitation spectrum and (ii) the integral of the MIR excitation spectrum [Fig. 6(b)]. The resulting fraction is 0.21%, corresponding to an absorbed energy of 1.1 nJ per laser shot.

The model predicts unphysically high temperatures shortly after the excitation pulse due to the assumption of an infinitesimally small point-like heat source. However, for the diffusion times corresponding to the laser repetition periods (i.e., 10-200 μs for 100-5 kHz) and deposited energies considered here, the model is regarded as a valid approximation. As is customary, the effect of heat accumulation during the laser pulse train is expressed as the rise in the offset temperature immediately before the next excitation pulse.[18,44] If this rise in offset temperature is high enough, the molecules in the lipid layer can get distorted and the layer can undergo a phase transition altering the measured VSFG spectrum. The high temperatures immediately following the excitation pulse are not expected to lead to distorted VSFG spectra, as the VIS-MIR time delay is on the sub-ps scale, which is too short for macromolecular rearrangements. We also note that the pulse energies and peak intensities used in our experiments are much smaller than in typical BB-VSFG spectroscopy experiments employing 1-kHz excitation sources. The equation for the temperature rise [Eq. (10) in Ref. 44],

$$\Delta T = \lim_{Np \to \infty} \frac{Q_{3D}}{\rho c_p \sqrt{(4\pi\kappa/f_L)^3}} \sum_{N=1}^{Np} \frac{1}{\sqrt{N^3}}, \quad (1)$$

where ρ, c_p, and κ are the mass density, specific heat capacity, and thermal diffusivity of CaF$_2$, respectively, f_L is the laser repetition frequency, $Q_{3D} = 2 \times$ (absorbed laser energy) is the heat source, and N is the pulse number. Figure 6(c) summarizes the predictions of Eq. (1) as a function of laser repetition rate and supports the experimental findings discussed above: the temperature accumulation effects are negligible under the conditions of our BB-VSFG experiments.

CONCLUSION

We employed a high repetition rate BB-VSFG spectrometer with continuously adjustable repetition rate to study possible laser average power induced temperature effects on the measured VSFG spectra of PC. The VSFG spectra were

recorded in four polarization combinations at the CaF$_2$/air interface. The signal-to-noise ratio (SNR) and the spectral distortions were studied at four repetition rates (5, 10, 50, and 100 kHz) at constant MIR and VIS pulse energy and number of laser shots. Our signal-to-noise ratios at 5 kHz approached those in the literature[3,42,43] despite the two orders of magnitude lower average excitation powers than in previous studies. The spectral amplitude of the C–H stretching bands was monitored as a function of time in order to detect any time-dependent temperature effects. The experimental results indicate that the influence of thermal effects on the vibrational signatures was negligible in all cases. This result is in agreement with a simple 3-dimensional analytical heat diffusion model treating the heat accumulation effects during the laser pulse train.

The findings suggest that the unique light source used in this study consisting of only a two-stage OPA and a narrow-band VIS pulse generator driven by a single pump laser[17] provides a promising tool for high repetition rate BB-VSFG studies with improved spectral resolution and sensitivity compared to traditional Ti:sapphire laser based, low repetition rate spectrometers.

SUPPLEMENTARY MATERIAL

See supplementary material for the modeling results on the vibrational spectra of the studied natural lipid bilayers at the CaF$_2$/air interface.

ACKNOWLEDGMENTS

[1] H.-F. Wang, L. Velarde, W. Gan, and L. Fu, Annu. Rev. Phys. Chem. **66**, 189 (2015).
[2] C. Weeraman, A. K. Yatawara, A. N. Bordenyuk, and A. V. Benderskii, J. Am. Chem. Soc. **128**, 14244 (2006).
[3] E. L. Hommel, G. Ma, and H. C. Allen, Anal. Sci. **17**, 1325 (2001).
[4] X. D. Zhu, H. Suhr, and Y. R. Shen, Phys. Rev. B **35**, 3047 (1987).
[5] Y. R. Shen, Nature **337**, 519 (1989).
[6] G. M. Cooper and R. E. Hausman, *The Cell: A Molecular Approach* (ASM Press, Washington, DC, USA, 2009).
[7] W. Liu, Z. Wang, L. Fu, R. M. Leblanc, and E. C. Y. Yan, Langmuir **29**, 15022 (2013).
[8] B. Li, X. Lu, X. Han, F.-G. Wu, J. N. Myers, and Z. Chen, J. Phys. Chem. C **118**, 28631 (2014).
[9] G. Ma and H. C. Allen, Langmuir **22**, 5341 (2006).
[10] W. Sung, S. Seok, D. Kim, C. S. Tian, and Y. R. Shen, Langmuir **26**, 18266 (2010).
[11] Y. Nojima, Y. Suzuki, and S. Yamaguchi, J. Phys. Chem. C **121**, 2173 (2017).
[12] J. F. D. Liljeblad, V. Bulone, M. W. Rutland, and C. M. Johnson, J. Phys. Chem. C **115**, 10617 (2011).
[13] B. Li, X. Li, Y.-H. Ma, X. Han, F.-G. Wu, Z. Guo, Z. Chen, and X. Lu, Langmuir **32**, 7086 (2016).
[14] C. S. Tian and Y. R. Shen, Surf. Sci. Rep. **69**, 105 (2014).
[15] O. Isaienko and E. Borguet, Opt. Express **20**, 547 (2012).
[16] D. K. Hore, J. L. King, F. G. Moore, D. S. Alavi, M. Y. Hamamoto, and G. L. Richmond, Appl. Spectrosc. **58**, 1377 (2004).
[17] Z. Heiner, V. Petrov, and M. Mero, APL Photonics **2**, 066102 (2017).
[18] E. H. G. Backus, D. Bonn, S. Cantin, S. Roke, and M. Bonn, J. Phys. Chem. B **116**, 2703 (2012).
[19] Z. Wang, J. A. Carter, A. Lagutchev, Y. K. Koh, N.-H. Seong, D. G. Cahill, and D. D. Dlott, Science **317**, 787 (2007).
[20] J. Liu and J. C. Conboy, J. Am. Chem. Soc. **126**, 8894 (2004).
[21] H.-L. Wu, Y. Tong, Q. Peng, N. Li, and S. Ye, Phys. Chem. Chem. Phys. **18**, 1411 (2016).
[22] M. J. Hope, M. B. Bally, G. Webb, and P. R. Cullis, Biochim. Biophys. Acta, Biomembr. **812**, 55 (1985).
[23] X. Zhang, X. Wang, and J. D. Miller, Surf. Innovations **3**, 39 (2015).
[24] E. Kalb, S. Frey, and L. K. Tamm, Biochim. Biophys. Acta, Biomembr. **1103**, 307 (1992).
[25] R. Tero, Materials **5**, 2658 (2012).
[26] P. B. Miranda and Y. R. Shen, J. Phys. Chem. B **103**, 3292 (1999).
[27] S. J. Kweskin, K. Komvopoulos, and G. A. Somorjai, Langmuir **21**, 3647 (2005).
[28] R. Lu, W. Gan, B.-h. Wu, H. Chen, and H.-f. Wang, J. Phys. Chem. B **108**, 7297 (2004).
[29] X. Zhuang, P. B. Miranda, D. Kim, and Y. R. Shen, Phys. Rev. B **59**, 12632 (1999).
[30] A. G. Lambert, P. B. Davies, and D. J. Neivandt, Appl. Spectrosc. Rev. **40**, 103 (2005).
[31] A. D. Curtis, S. R. Burt, A. R. Calchera, and J. E. Patterson, J. Phys. Chem. C **115**, 11550 (2011).
[32] A. D. Curtis, S. B. Reynolds, A. R. Calchera, and J. E. Patterson, J. Phys. Chem. Lett. **1**, 2435 (2010).
[33] A. Lagutchev, S. A. Hambir, and D. D. Dlott, J. Phys. Chem. C **111**, 13645 (2007).
[34] J. E. Laaser, W. Xiong, and M. T. Zanni, J. Phys. Chem. B **115**, 2536 (2011).
[35] F. Y. Shalhout, S. Malyk, and A. V. Benderskii, J. Phys. Chem. Lett. **3**, 3493 (2012).
[36] L. Velarde and H.-F. Wang, Phys. Chem. Chem. Phys. **15**, 19970 (2013).
[37] C. Weeraman, S. A. Mitchell, R. Lausten, L. J. Johnston, and A. Stolow, Opt. Express **18**, 11483 (2010).
[38] I. V. Stiopkin, H. D. Jayathilake, C. Weeraman, and A. V. Benderskii, J. Chem. Phys. **132**, 234503 (2010).
[39] R. Lu, W. Gan, B.-h. Wu, Z. Zhang, Y. Guo, and H.-f. Wang, J. Phys. Chem. B **109**, 14118 (2005).
[40] R.-J. Feng, X. Li, Z. Zhang, Z. Lu, and Y. Guo, J. Chem. Phys. **145**, 244707 (2016).
[41] K. Tian, B. Zhang, S. Ye, and Y. Luo, J. Phys. Chem. C **119**, 16587 (2015).
[42] G. Ma, J. Liu, L. Fu, and E. C. Y. Yan, Appl. Spectrosc. **63**, 528 (2009).
[43] E. C. Y. Yan, L. Fu, Z. Wang, and W. Liu, Chem. Rev. **114**, 8471 (2014).
[44] R. Weber, T. Graf, P. Berger, V. Onuseit, M. Wiedenmann, C. Freitag, and A. Feuer, Opt. Express **22**, 11312 (2014).
[45] R. Weber, T. Graf, P. Berger, V. Onuseit, M. Wiedenmann, C. Freitag, and A. Feuer, Opt. Express **22**, 28232 (2014).
[46] F. Picard, T. Buffeteau, B. Desbat, M. Auger, and M. Pézolet, Biophys. J. **76**, 539 (1999).